A Single-Channel THz Imaging System for Biomedical Applications

Tonny Rubæk[1], ***Robin N. Dahlbäck***[2], ***Andreas Fhager***[1], ***Mikael Persson***[1], and ***Jan Stake***[2]

[1] Division of Signal Processing and Biomedical Engineering, Department of Signals and Systems
Chalmers University of Technology
SE-41296 Gothenburg, Sweden
rubaek@chalmers.se, andreas.fhager@chalmers.se, mikael.persson@chalmers.se

[2] Terahertz and Millimetre Wave Laboratory, Department of Microtechnology and Nanoscience – MC2
Chalmers University of Technology
SE-41296 Gothenburg, Sweden
dahlback@chalmers.se, jan.stake@chalmers.se

Abstract

Due to technological advances, imaging in the THz-range of the electromagnetic spectrum is currently emerging as an interesting tool for security, safety, and biomedical applications. In this paper, a THz imaging system designed for biomedical analysis is described. The system consists of a pair of antennas operating in transmission mode at 335 GHz. The antennas can be moved independently of each other and a tomographic imaging algorithm is used to reconstruct the images.

1 Introduction

In recent years, advances in the development of hardware in the THz region of the electromagnetic spectrum (ranging from 300 GHz to 3 THz) has made imaging and spectroscopy with THz waves a viable tool for medical applications [1–3] such as cancer diagnostics, dental imaging, and wound monitoring [4–6].

At THz frequencies, the absorption caused by the water content of the biological tissues is governing the interaction between the electromagnetic waves and the tissue. This allows for easily identifying tissues with different water content, e.g., healthy and cancerous tissue [7, 8]. It does, however, also severely limits the penetration, implying that only the outermost few fractions of a mm of most soft tissues can be examined [4]. For tissues with a low content of water, such as teeth and bone, the penetration depth is much greater [3, 9]. A number of biomedically interesting molecules also have resonances in the THz part of the frequency spectrum [10, 11]. This implies that apart from classical imaging, spectroscopy is also an interesting biomedical application of THz.

THz imaging today is most commonly performed using pulsed THz imaging in which a short pulse (having a wide bandwidth) is used to image the sample. The imaging system may be operating either with transmission measurements with the sample under investigation positioned between the transmitting and receiving antennas [12], or in reflection mode with the transmitter and receiver positioned on the same side of the sample [13, 14].

In this paper, a continuous-wave system which is currently being developed at Chalmers University of Technology is described. In such systems, the information which is contained in the multiple frequencies of the broadband imaging system must be retrieved by combining different transmitter and receiver combinations. This paper includes a description of the THz hardware and a description of the tomographic imaging algorithm.

978-1-4244-6051-9/11/$26.00

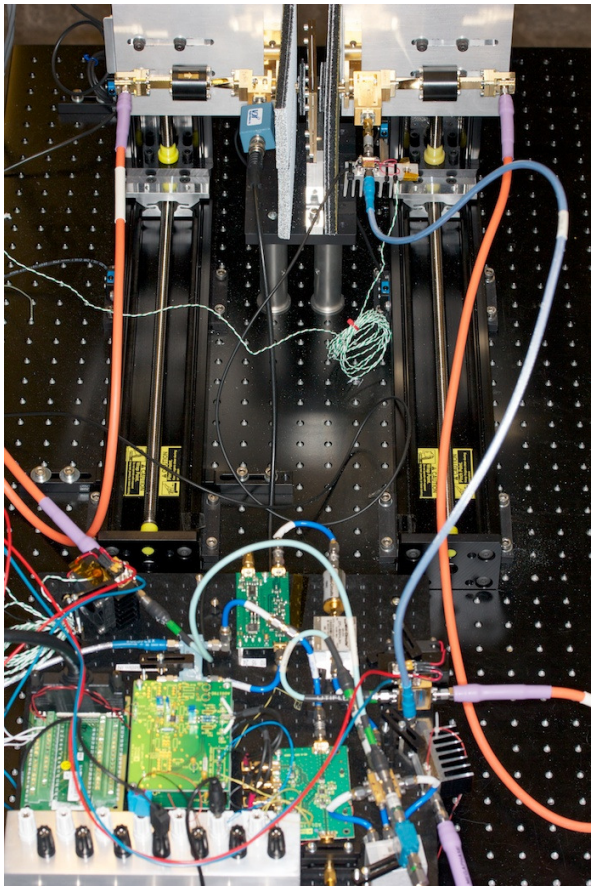

Figure 1: Photo of the imaging system. The IF hardware can be seen in the bottom of the photo while the frequency doublers and antennas are mounted on the movable axes in the top of the photo.

Figure 2: Photo of the antennas used in the system. The antennas are open-ended waveguides and absorbers have been mounted behind the antennas to minimize the effects of standing waves.

2 System Design

A photo of the system is shown in Fig. 1. The system consists of three parts: A high-frequency circuit capable of transmitting a CW signal on the transmitting channel while measuring the resulting amplitude and phase on the receiving channel; a mechanical setup capable of scanning the transmit and receive antennas independent of each other at opposite sides of the sample to be investigated; and finally a computer which controls the data acquisition process.

The antennas used in the system are simple open-ended waveguides based on standard rectangular WR-2.8 waveguides. A photo of the antennas is shown in Fig. 2. To minimize the effects of standing waves in the imaging domain, absorbers have been placed behind and around the antennas. These can be seen as the gray and black slabs in Fig. 2. By surrounding the antennas with absorbers in this manner, the influence of the surroundings is effectively eliminated and the antennas behaves as if they are positioned in free space.

The antennas are characterized by a rather broad radiation pattern. The 3 dB beam width in the farfield is approximately 110° by 70° and although the antennas are not used in the farfield, this gives a good indication of the width of the beam of the antennas. Although such a broad beam is usually avoided in

wideband imaging systems, the broad beam is advantageous when doing CW imaging since it allows for the transmitter and receiver to see the same region of the sample under test from multiple angles. Something which is not easily achieved with antennas with a narrow beam.

3 Imaging Algorithm

In the imaging system, a tomographic algorithm is applied for creating the images. The measured complex signal $S_{r,t}$ for a given position of the transmit and receive antennas (indicated by the subscript r,t) can be divided into two components: One originating from the incident field and one from the scattered field. The incident field is the field which is present in the system when there is no sample in the system, and the scattered field is the field which arises when a sample is positioned in the system. The signal can thus be expressed as:

$$S_{r,t}^{\text{tot}} = S_{r,t}^{\text{inc}} + S_{r,t}^{\text{sct}} \tag{1}$$

wherein $S_{r,t}^{\text{tot}}$ is the total measured signal, $S_{r,t}^{\text{inc}}$ is the part of the signal originating from the incident field, and $S_{r,t}^{\text{sct}}$ is the part of the signal originating from the scattered field.

By introducing the object function

$$O(\boldsymbol{r}) = \Delta\sigma(\boldsymbol{r}) - i\omega\Delta\epsilon(\boldsymbol{r}) \tag{2a}$$

the scattered field from a given object can be expressed as

$$\boldsymbol{E}^{\text{sct}} = i\omega\mu_0 \int_V \bar{\bar{\boldsymbol{G}}}(\boldsymbol{r}, \boldsymbol{r'}) \cdot \boldsymbol{E}^{\text{tot}}(\boldsymbol{r'}) O(\boldsymbol{r'}) \, \mathrm{d}\boldsymbol{r'}. \tag{2b}$$

In these expressions $\boldsymbol{r}$ and $\boldsymbol{r'}$ are position vectors, $\bar{\bar{\boldsymbol{G}}}$ is the dyadic Green's function, and $\boldsymbol{E}^{\text{sct}}$ and $\boldsymbol{E}^{\text{tot}}$ are the scattered and total electric field, respectively. The object function O is given by the contrast in conductivity σ and permittivity ϵ between the object and the background, i.e.,

$$\Delta\sigma(\boldsymbol{r}) = \sigma(\boldsymbol{r}) - \sigma_{\text{bg}} \tag{3a}$$

and

$$\Delta\epsilon(\boldsymbol{r}) = \epsilon(\boldsymbol{r}) - \epsilon_{\text{bg}}. \tag{3b}$$

By application of the reciprocity theorem it can be shown that the change in the measured signal caused by the presence of a scatterer can be expressed as

$$S_{r,t}^{\text{sct}} = \alpha \int_V \boldsymbol{E}^{\text{trans}}(\boldsymbol{r'}) \cdot \boldsymbol{E}^{\text{rec}}(\boldsymbol{r'}) O(\boldsymbol{r'}) \, \mathrm{d}\boldsymbol{r'} \tag{4}$$

wherein α is a constant which is dependent on various parameters of the system setup, such as how the antennas are fed. The two fields $\boldsymbol{E}^{\text{trans}}(\boldsymbol{r'})$ and $\boldsymbol{E}^{\text{rec}}(\boldsymbol{r'})$ are the fields at the point $\boldsymbol{r'}$ when the transmitting or the receiving antenna, respectively, are transmitting.

Thus, the expression in (4) allows for setting up an equation system which can be solved for the unknown distribution of the object function. For small targets or targets with low contrast, the expression in (4) can be solved as a set of linear equations wherein the fields $\boldsymbol{E}^{\text{trans}}(\boldsymbol{r'})$ and $\boldsymbol{E}^{\text{rec}}(\boldsymbol{r'})$ are assumed to be equal to those of the empty system. By discretizing the volume in which the sample under investigation is positioned and scanning the transmitting and receiving antennas to several different locations, the matrix equation

$$\underline{\underline{E}}\,\underline{O} = \underline{S} \tag{5}$$

can be constructed. Herein $\underline{\underline{E}}$ is a matrix consisting of the products of the fields for each of the cells of the discretized volume, $\underline{O}$ is a column vector holding the unknown values of the object function, and $\underline{S}$ is a column vector holding the measured signals.

4 Conclusion

A THz imaging is being developed at Chalmers University of Technology. The imaging system works at a single frequency (335 GHz) and is designed for imaging of biological samples, e.g., histopathology samples, in transmission mode. The system has a single transmitter and a single receiver which can be mechanically scanned independently of each other.

At the conference, the system will be described in details and images of different biological and non-biological targets will be presented.

References

[1] P. Siegel, "Terahertz technology in biology and medicine," *Microwave Theory and Techniques, IEEE Transactions on*, vol. 52, no. 10, pp. 2438–2447, 2004. [Online]. Available: 10.1109/TMTT.2004.835916

[2] D. Woolard, R. Brown, M. Pepper, and M. Kemp, "Terahertz frequency sensing and imaging: A time of reckoning future applications?" *Proceedings of the IEEE*, vol. 93, no. 10, pp. 1722–1743, 2005.

[3] E. Pickwell and V. P. Wallace, "Biomedical applications of terahertz technology," *Journal of Physics D: Applied Physics*, vol. 39, no. 17, pp. R301–R310, 2006.

[4] R. M. Woodward, V. P. Wallace, D. D. Arnone, E. H. Linfield, and M. Pepper, "Terahertz pulsed imaging of skin cancer in the time and frequency domain," *Journal of Biological Physics*, vol. 29, no. 2, p. 257259, 2003.

[5] Z. D. Taylor, R. S. Singh, M. O. Culjat, J. Y. Suen, W. S. Grundfest, H. Lee, and E. R. Brown, "Reflective terahertz imaging of porcine skin burns," *Optics Letters*, vol. 33, no. 11, pp. 1258–1260, Jun. 2008.

[6] J. Son, "Terahertz electromagnetic interactions with biological matter and their applications," *Journal of Applied Physics*, vol. 105, no. 10, p. 102033, 2009.

[7] A. J. Fitzgerald, V. P. Wallace, M. Jimenez-Linan, L. Bobrow, R. J. Pye, A. D. Purushotham, and D. D. Arnone, "Terahertz pulsed imaging of human breast tumors," *Radiology*, vol. 239, no. 2, p. 533, 2006.

[8] H. Hoshina, A. Hayashi, N. Miyoshi, F. Miyamaru, and C. Otani, "Terahertz pulsed imaging of frozen biological tissues," *Applied Physics Letters*, vol. 94, no. 12, p. 123901, 2009.

[9] D. Arnone, C. Ciesla, M. Pepper *et al.*, "Terahertz imaging comes into view," *Physics World*, vol. 4, p. 3540, 2001.

[10] H. H. Mantsch and D. Naumann, "Terahertz spectroscopy: The renaissance of far infrared spectroscopy," *Journal of Molecular Structure*, vol. 964, no. 1-3, pp. 1–4, Feb. 2010.

[11] T. Globus, "Optical characteristics of biological molecules in the terahertz gap," in *Proceedings of SPIE*, Philadelphia, PA, USA, 2004, pp. 1–10.

[12] C. Chiu, H. Chen, Y. Huang, W. Lee, Y. Hwang, H. Huang, and C. Sun, "All-terahertz fiber-scanning near-field microscopy," *Optics Letters*, vol. 34, no. 7, pp. 1084–1086, 2009.

[13] R. M. Woodward, B. E. Cole, V. P. Wallace, R. J. Pye, D. D. Arnone, E. H. Linfield, and M. Pepper, "Terahertz pulse imaging in reflection geometry of human skin cancer and skin tissue," *Physics in Medicine and Biology*, vol. 47, p. 38533863, 2002.

[14] C. B. Reid, E. Pickwell-MacPherson, J. G. Laufer, A. P. Gibson, J. C. Hebden, and V. P. Wallace, "Accuracy and resolution of THz reflection spectroscopy for medical imaging," *Physics in Medicine and Biology*, vol. 55, no. 16, pp. 4825–4838, 2010.